Talanta 85 (2011) 2553–2561

Contents lists available at ScienceDirect

Talanta

journal homepage: www.elsevier.com/locate/talanta

Characterization of BSA unfolding and aggregation using a single-capillary viscometer and dynamic surface tension detector

Emilia Bramanti[a,*], Carlo Ferrari[b], Valeria Angeli[a], Massimo Onor[a], Robert E. Synovec[c]

[a] National Research Council of Italy, C.N.R., Istituto di Chimica dei Composti Organo Metallici-ICCOM-UOS Pisa, Area di Ricerca, Via G. Moruzzi 1, 56124 Pisa, Italy
[b] National Research Council of Italy, C.N.R., Istituto Nazionale di Ottica, INO – UOS Pisa, Area di Ricerca, Via G. Moruzzi 1, 56124 Pisa, Italy
[c] Department of Chemistry, Box 351700, Center for Process Analytical Chemistry, University of Washington, Seattle, WA 98195, USA

ARTICLE INFO

Article history:
Received 11 April 2011
Received in revised form 5 August 2011
Accepted 6 August 2011
Available online 12 August 2011

Keywords:
Denaturation
β-Aggregation
Proteins
Viscosity
Surface tension
DSTD
Bovine serum albumin
FTIR conformational analysis

ABSTRACT

A dynamic surface tension detector (DSTD) has been equipped with an additional pressure sensor for simultaneous viscosity measurements, as a detector for flow injection analysis. The viscosity measurement is based on a single capillary viscometer (SCV) placed in parallel configuration with the DSTD. The viscometer in the optimized conditions consists of a PEEK capillary (i.d. = 0.25 mm, L = 75 cm) kept at constant temperature using a thermostatic bath, which leads on the two sides to the two arms of a differential piezoelectric pressure transducer with a range of 0–35 psi. The DSTD, described previously, measures the changing pressure across the liquid/air interface of 2 μL drops repeatedly forming at the end of a capillary.

SCV performance has been evaluated by measuring dynamic viscosity of water/glycerol mixtures analysed in flow injection and comparing the results with the values reported in the literature. The detection limits of SCV and DSTD, calculated as 3σ of the blank, were 0.012 cP and 0.6 dyn cm^{-1}, respectively.

The FI-SCV-DSTD system has been applied to the study of temperature-induced denaturation/aggregation process in bovine serum albumin (BSA).

The results have been supported and discussed with respect to BSA conformational analysis performed using Fourier Transform infrared spectroscopy.

1. Introduction

Reliable and accurate methods for characterizing viscosity and surface tension changes of proteins caused by the alteration of their composition or conformation can have significant clinical and biotechnological utility [1,2]. The measurement of viscosity is one of the most common and important means of quality control [3,4]. Surface tension, as well, not only determines the quality of many products resulting from different industries (coatings, paints, detergents, cosmetics and agrochemicals), but also affects some important steps in production processes (*e.g.* catalysis, adsorption, distillation and extraction).

While most conventional methods determine viscosity and surface tension in a relative manner with two completely different sets of experimental instrumentation, very few methods lead to the simultaneous detection of viscosity and surface tension for materials of interest. One of these is based on the surface light scattering technique [5] and it has been applied to various compounds. Another one is based on the oscillating drop methods [6,7]. Both these methods require a complex apparatus and are not straightforwardly applicable as detectors of flow injection and liquid chromatographic systems, nor for protein rheological characterization. The third apparatus, named a survismeter, has been applied to the study of proteins, but it is not suitable as an on-line detector [8–10]. The simultaneous measurement of viscosity and surface tension of proteins is of particular interest for two important reasons: (i) small amounts of sample are generally available (0.01–0.1 mg) and (ii) protein structure changes induced by several parameters like temperature may vary in the minute range, thus the sequential measure of surface tension and viscosity may correspond to different structures.

In this work we propose a simple flow injection system able to simultaneously measure viscosity and surface tension on small amounts of proteins (about 1 mg), in a very short time (about 3 min).

In previous studies, we have developed a detector capable of measuring dynamic surface tension, *i.e.*, a dynamic surface tension detector (DSTD). The DSTD is a drop-based analyser that, when used as a chromatographic detector, provides real-time dynamic surface pressure measurements of components as they elute. The DSTD has evolved from an optical measurement-based instrument to a pressure sensor-based instrument, and has been used in conjunction with flow injection analysis (FIA) and high performance liquid

* Corresponding author. Tel.: +39 050 3152293; fax: +39 050 315 2555.
E-mail address: bramanti@pi.iccom.cnr.it (E. Bramanti).

0039-9140/$ – see front matter © 2011 Elsevier B.V. All rights reserved.
doi:10.1016/j.talanta.2011.08.009

chromatography (HPLC) [11–18]. More recently, a novel DSTD calibration procedure has been presented and applied, based on a dual-mobile phase calibration procedure that allows the analyst to apply different mobile phases for the analyte (*e.g.* denatured protein) and the calibration standard [19–21].

In this report, the DSTD has been equipped with an additional pressure sensor for simultaneous viscosity measurements for FIA and HPLC. The viscosity measurement is based on a single capillary viscometer (SCV) design, placed in parallel configuration with the DSTD, similar to that described by Malihi et al. [22]. The viscometer, in the optimized conditions, consists of a PEEK capillary kept at constant temperature using a thermostatic bath, which leads on the two stainless steel membrane sides of a differential piezoelectric pressure transducer. First, in this report, the SCV performance has been evaluated by measuring dynamic viscosity of water/glycerol mixtures analysed in flow injection and the results have been compared with the values reported in the literature.

Second, the FIA-SCV-DSTD instrumental system has been used to study the effect of viscosity on DSTD signal. Third, this instrumental system has been applied to the study of temperature-induced denaturation/aggregation process in bovine serum albumin (BSA). The results are then supported and discussed with respect to BSA conformational analysis performed using Fourier Transform infrared spectroscopy (FTIR).

2. Experimental

2.1. Materials and solutions

Bovine serum albumin (BSA, A-0281) and sodium chloride (99.5% purity) were purchased from Aldrich–Sigma–Fluka Chemical Co. (Milan, Italy). All materials were used without further purification. Phosphate buffer solution (PBS, 50 mM pH 7.4 or 6.0) was prepared from monobasic monohydrate sodium phosphate and dibasic anhydrous potassium phosphate (BDH Laboratory Supplies, Poole, England). All solutions were prepared with water deionized (18.2 MΩ × cm) with a Milli-Q system (Millipore, Bedford, MA, USA). Viscous solutions were prepared with mass ratios of glycerol (4094, Merck 87%) to water (glycerol:water, mass ratio). BSA was prepared in 25 mM pH 7.4 or 6.0 PBS and injected at the indicated times after incubation at 21, 60, or 80 °C in a thermostatic bath. Several experiments were performed denaturing BSA in 50 mM pH 7.4, 8 M urea (Sigma–Aldrich U-0631). All sample concentrations are given as injected; the protein amounts at the SCV and DSTD detector are 42% and 10% of the total injected amount (injected concentration × 100 μL loop volume) due to flow splitting (see below).

2.2. Instrumental set-up

The DSTD is based upon a repetitive growing drop method, implementing a pressure sensor (P305D-20-2369, diaphragm 3-36, Validyne Northridge, CA, USA) where the pressure signal is dependent upon surface tension properties of a given sample. The pressure sensor, mounted in the sidearm off the main flow of a capillary, measures the internal pressure of the growing drops relative to atmospheric pressure. The flow passes through a short capillary, forming drops at a specially designed sensing capillary tip. The drops are detached by an air burst supplied by a solenoid valve (pneumatic detachment) at a preset rate [11–18].

A detailed schematic of the FIA-SCV-DSTD system is shown in Fig. 1A. A Jasco PU2085 Plus microbore isocratic pump (Milan, Italy) was operated at a flow rate of 450 μL/min. Samples were introduced via a Rheodyne 7125 injector (Rheodyne, Cotati, CA, USA). A poly(etheretherketone) (PEEK) injection loop of 100 μL of tubing (Upchurch, Oak Harbor, WA, USA) was used for all experiments.

The DSTD configuration is identical to that detailed in our previous work [20,23]. Pneumatic detachment of DSTD drops was performed at a rate of 0.5 Hz, corresponding to 1.5 μL drops at 45 μL/min (resulting in 2-s drop times), using a Skinner solenoid valve (MBD002, Skinner Valve, New Britain, CT, USA).

The viscometer in the optimized conditions consists of a PEEK capillary (i.d. = 0.25 mm, L = 75 cm) kept at constant temperature set by a thermostatic bath. The pressure drop is measured between the two ends of the PEEK capillary by another differential piezoelectric pressure transducer (P305D-20-2369, diaphragm 3-36, Validyne Northridge, CA, USA) with a range of 0–35 psi. The connection between each end of the PEEK thermostated capillary and the two sides of the pressure transducer membrane was performed by PEEK tubing (Fig. 1B).

Calibration of the SCV pressure sensor was performed by connecting a burette filled with distilled water with one arm of the differential pressure sensor. The second arm of the sensor was equilibrated relative to atmospheric pressure. Three clusters of measurements (signal averaged for 1 min) were performed at three different levels with respect to the pressure sensor (199, 508 and 995 mm). Pressure sensor signal in volts was plotted as a function of the pressure calculated on the basis of the height of water column. Fitting of data was linear (slope = −0.195 V/kPa, intercept = −0.123, R = 0.999) with a difference between the fitting curve and experimental data <3 mV, which corresponded to 0.015 kPa or 1.5 mm H_2O.

A polynomial fitting equation ($-0.5998 - 4.9417V + 0.21416V^2 + 0.068501V^3$, where V is the signal in volts of the transducer) was employed to convert the differential pressure sensor signal in volts into differential pressure values (P, kPa).

All data were collected at 20 kHz with a personal computer (850 MHz Pentium, Intel, Santa Clara, CA, USA) equipped with a data acquisition card (AT-MIO-16XE-50, National Instruments, Austin, TX, USA). The data were averaged from 20,000 points/s to 50 points/s prior to saving and subsequent analysis. Data collection was completed using LabVIEW (version 6.0, National Instruments) with programs written in-house. Subsequent data analysis was performed using Origin 8.0 (OriginLab, Adalta, Arezzo, Italy). Water/glycerol mixtures (1–50% w/w) were injected in various conditions, varying L, r and temperature, where L and r are the length and radius of the measure PEEK tubing, respectively. Dynamic viscosity of the injected analyte solution was calculated using a written-in house LabVIEW program (LabVIEW 6.1, National Instruments, Milan, Italy) on the basis of integrated area of flow injection peak (A) and the Hagen–Poiseuille law:

$$\eta = \frac{A\pi r^4}{8V_{\text{inj}}L} \tag{1}$$

where V_{inj} is the injected volume. Accuracy of viscosity measurement was performed by correlating viscosity values found by injecting water/glycerol mixtures (1–50%, w/w) in the system with values known from the literature (see Supplementary Data, Fig. S1 and Table S1) [24]. The detection limit calculated as 3σ of the blank was 0.012 cP. Repeated experiments showed good repeatability (CV% < 1%).

If we let η_0 be the viscosity of the pure solvent and η be the viscosity of a solution using that solvent, specific viscosity, η_{sp}, is defined as:

$$\eta_{\text{sp}} = \frac{\eta - \eta_0}{\eta_0} = \eta_{\text{r}} - 1 \tag{2}$$

where η_{r} is the relative viscosity (η/η_0).

According to the Huggins equation [25], in dilute solution η_{sp} is proportional to the concentration of macromolecules in solution,

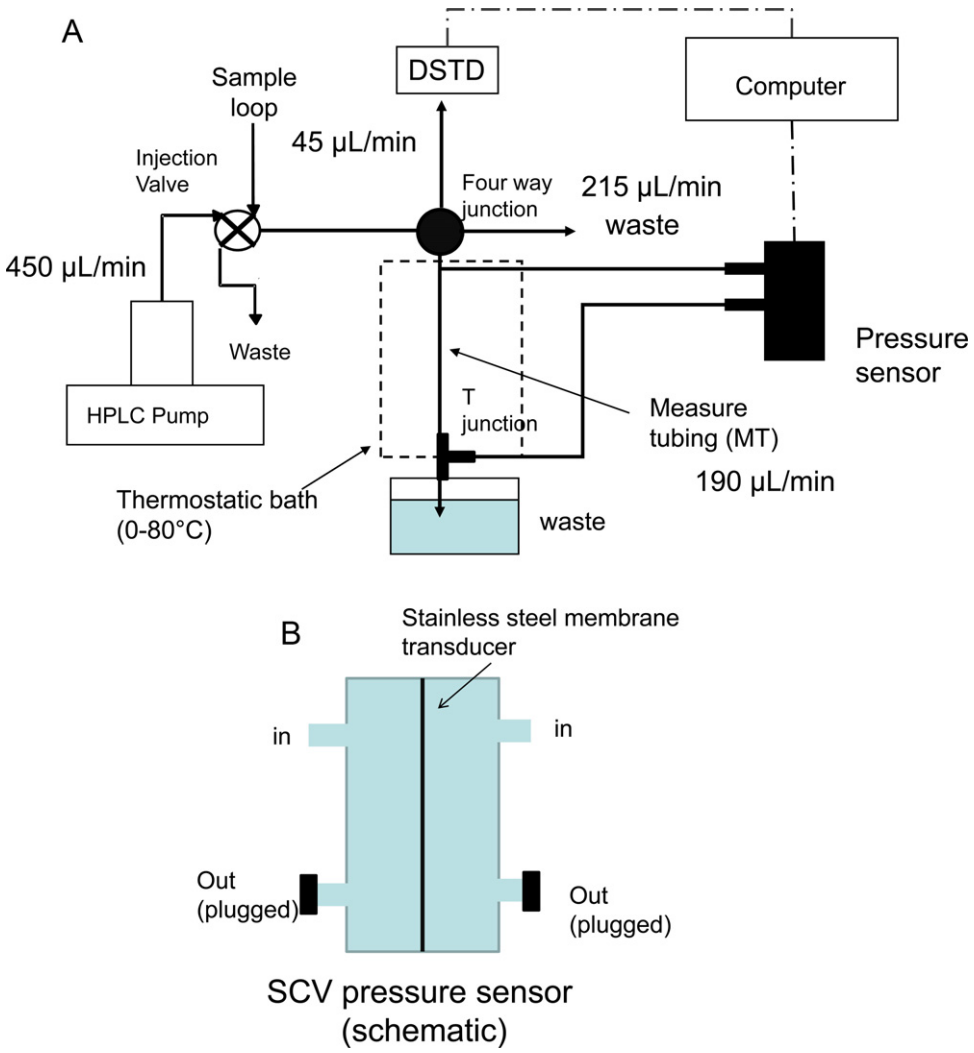

Fig. 1. (A) FIA-SCV-DSTD instrument configuration. The HPLC pump transfers the sample from the injector to the SCV and DSTD. The flow splitter delivers 45 μL/min of the total flow (0.45 mL/min) to the DSTD and 190 μL/min to the SCV detector. A schematic diagram of the DSTD and operating conditions for it have been previously reported [19,20,23]. Operating conditions for SCV detector were the following: measure tubing length 20, 40, 75 cm (i.d. = 0.25 mm), 30 cm (i.d. = 0.17 mm), 50 cm (i.d. = 0.5 mm); flow = 15, 30,45, 60, 80, 100 μL/min; temperature of measure tubing = 3, 5, 20, 22.5, 40 °C. (B) Schematic of SCV pressure sensor.

c, and the proportionality constant is called the intrinsic viscosity $[\eta]$:

$$\eta_{sp} \cong [\eta]\, c \tag{3}$$

The intrinsic viscosity, molecular weight, M, and hydrodynamic radius, R_e, are related as follows:

$$[\eta] = \frac{10\pi N_A}{3M} R_e^3 \tag{4}$$

Since N_A is the Avogadro number, if M is known, R_e can be derived from $[\eta]$ measurement. R_e measurement is especially useful for protein characterization. For large random coils $R_e \cong 0.88\, R_G$, where R_G is the radius of gyration of the molecule [25].

2.3. FTIR spectroscopy

Infrared spectra were recorded by using a Perkin-Elmer Spectrum One FTIR spectrophotometer, equipped with a universal ATR accessory and a TGS detector. After recording the background spectrum on 20 μL of PBS, sample spectra were obtained on 20 μL of each protein solution before and after thermal treatments. For each sample, 128 interferograms were recorded in order to obtain a suitable S/N ratio, averaged and Fourier-transformed to produce a spectrum with a nominal resolution of 4 cm^{-1}. The typical vapour band did not appear either in the spectra or in the second derivative.

Spectrum software (Perkin-Elmer) and a written-in house LabVIEW program for peak fitting were employed to run and process spectra, respectively. The LabVIEW program for peak fitting was based on a previous work [26,27]. Prior to curve processing, a straight baseline passing through the ordinates at 1800 and 1480 cm^{-1} was subtracted and spectra were normalized in the 1700–1600 cm^{-1} region. This approach was taken in order to avoid artefacts in absorptions near the limits of the region examined (1700–1600 cm^{-1}). Then, the second derivatives of the amide I band of the spectra examined (1700–1600 cm^{-1} region) were analysed in order to determine the starting data (number and position of Gaussian components) required for the deconvolution procedure. The choice of the amide I band for structural analysis is due to the very low contribution of the amino acid side chain absorptions present in this region [28], and to its higher intensity with respect to other amide modes. On the basis of the infrared assignment of amide components, assuming that the extinction coefficient is the same for all the secondary structures, the secondary structure composition can be obtained from the FTIR spectra. The values for the percentages of the different secondary structures were estimated by expressing the amplitude value of the bands assigned to each of

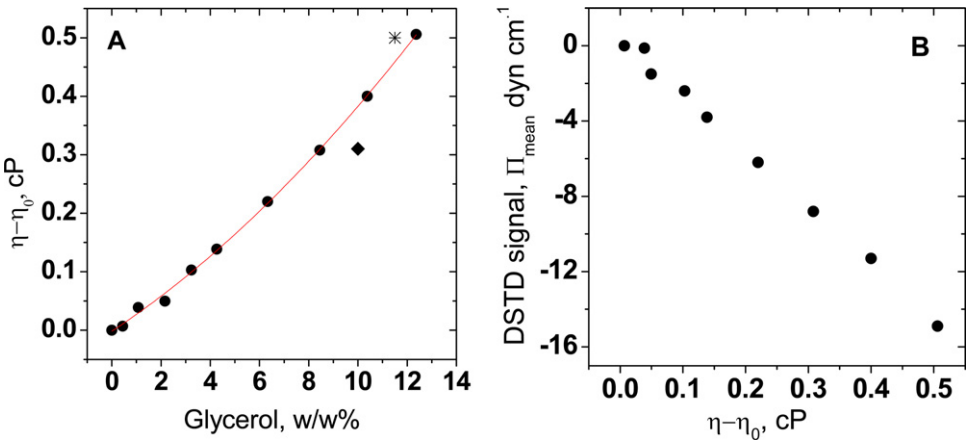

Fig. 2. (A) Viscosity values found ($\eta - \eta_0$) using on line SCV at 20 °C *vs.* glycerol concentration at SCV detector (R^2 = 0.9985, polynomial equation). Data available from the literature are indicated as an asterisk [30] and filled diamond [29]. (B) Correlation between surface pressure values processed from DSTD signals and viscosity measured on line with the SCV detector.

these structures as a fraction of the total sum of the amplitudes of the amide I components. While the general validity of the assumption above made about the extinction coefficients remains to be tested, the good correlation found between the secondary structure results obtained by FTIR approaches and X-ray crystallography indicated that this is a reasonable assumption [27].

3. Results and discussion

3.1. Simultaneous measurement of DSTD and viscosity signal of glycerol solutions

Fig. 2A shows the dynamic viscosity values, represented as ($\eta - \eta_0$), found using on line SCV at 20 °C as a function of glycerol concentration at SCV detector (*i.e.* corrected considering the flow splitting). The values found are in good agreement with data available from the literature [29,30]. Fig. 2B shows the correlation between surface pressure values processed from DSTD signals and relative viscosity measured on line with SCV detector. For glycerol/water solutions with relative viscosity higher than 0.04 cP we observed a linear decrease of surface pressure (slope = -30.3 ± 0.75 dyn/(cm × cP), R^2 = 0.9957), in agreement with previous observations [31].

3.2. Denaturation study of BSA: rheological properties and conformational changes

Serum albumin is the one of the most important blood proteins, and it is characterized by an overall oblate shape, and it consists of three domains (I, II, and III), each stabilized by an internal network of disulfide bonds and each bearing a number of ionizable groups with opposite signs [32]. Bovine serum albumin (BSA), molecular mass 66,500 Da, is built from 583 amino acid residues containing 20 Tyr and 35 cysteine residues, 34 of which are involved in 17 S–S bridge [32]. The secondary structure of native BSA is composed of 67% helix, 10% turn, and 23% extended chain, and no β-sheet is contained [32]. Modifications in the secondary as well as tertiary structures of BSA occur in dependence of pH, temperature, and various kinds of denaturants [33]. Foster reported BSA has several isomeric forms at different pH media that correspond to different α-helix contents. Conformers are classified as E (extended at pH 2.7, 35% α-helix), F (fast migration at pH 4.5, 45% α-helix), N (normal dominant form at neutral pH, 55% α-helix), B (basic form at pH 10, 48% α-helix) and A (aged at pH 10, 48% α-helix) [34].

The FIA-SCV-DSTD instrument was applied to the study of temperature-induced denaturation/aggregation process of BSA at physiological pH (pH 7.4) and at pH 6.0, a value closer to BSA isoelectric point (pH 4.5–5.0) at whom albumins are characterized by a maximum surface activity [21]. The choice of this pH value allowed us to study the trend of viscosity and surface tension as a function

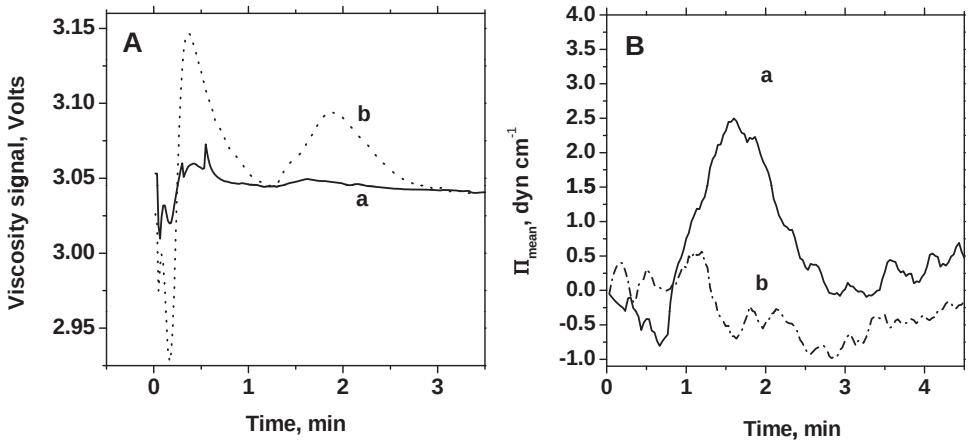

Fig. 3. Representative plots of the flow injection viscosity signal in volts from pressure sensor (A) and the Π_{mean} signal processed from DSTD raw (B). Ten mg/mL BSA in 25 mM PBS, pH 6.0 were injected at t = 0 (a) and after 60 min incubation at 80 °C (b).

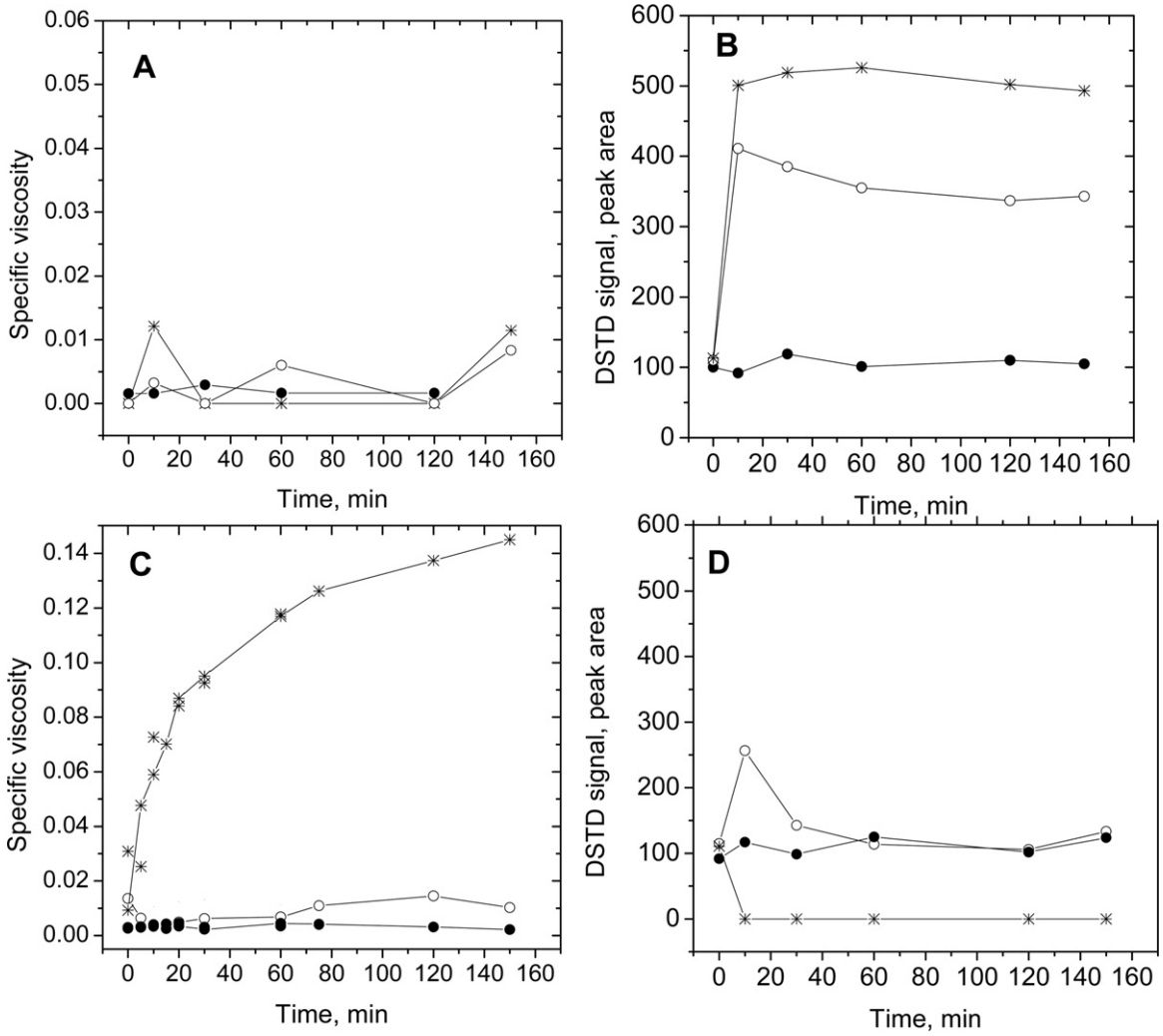

Fig. 4. Specific viscosity value (A and C) and DSTD peak area (B and D) of 10 mg/mL BSA in 25 mM PBS pH 7.4 (A and B) and 6.0 (C and D) as a function of incubation time at the three selected temperatures 21 (filled circles), 60 (open circles), and 80 °C (asterisks).

of heat denaturation getting closer to isoelectric pH, avoiding the drawback of DSTD saturation, which easily could occur at the pI. It is well established in the literature that for temperatures higher than 333 K (60 °C), the hydrodynamic diameter of BSA increased significantly, suggesting the appearance of large aggregates, due to the denaturation process. The temperature at which denaturation occurs is often referred to as the protein melting point, denoted by T_M. Previous literature data indicate that T_M for BSA is 63 °C [35].

Fig. 3 shows, as example, the flow injection peak of viscosity signal in volts from pressure sensor and the Π_{mean} signal processed from DSTD raw data, as previously reported [19]. The first peak in Fig. 3A is due to the pressure spike caused by the injection. The second peak is the analyte signal: absolute viscosity value is calculated on the basis of the peak area, as reported in Section 2. As far as DSTD data concern (Fig. 3B), in brief, Π_{mean} represents the surface pressure signal averaged over the last 25 points (0.5-s equivalent) at the end of the 2-s drop (average values from 1.5 to 2 s from each surface pressure plot).

Fig. 4 shows the specific viscosity value and DSTD peak area ($\Pi_{mean} \times$ min) as a function of incubation time of 10 mg/mL BSA in 25 mM PBS pH 7.4 and 6.0 at the three selected temperatures (21, 60, and 80 °C).

In order to discuss and correlate the surface tension and viscosity changes of BSA solutions with its temperature-induced changes in secondary structure, FTIR spectra were collected by sampling protein solutions at various incubation times and the conformational analysis was performed analysing the amide I region of FTIR spectra.

The detailed information on structural variations from the temperature-dependent IR spectra were obtained by employing a curve fitting method applied to the deconvolution of the amide I band mainly due to the C=O stretching vibration [26].

Fig. 5 shows some representative results of curve fitting for the FTIR spectra of BSA in the amide I region at pH 6 and 7.4 at 21 °C and after 150 min incubation at 80 °C.

The IR spectra of native BSA show a broad amide I band between 1700 and 1600 cm^{-1} that consists of overlapping component bands arising from different secondary structure elements (not shown for brevity). The second derivative spectra of BSA at 21 °C at pH 7.4 before heating is dominated by five bands at 1681, 1676, 1653, 1634 and 1623 cm^{-1} in the amide I region. The band at 1654 cm^{-1} is due to α-helical structures and around 1674 cm^{-1} is associated with turn structures [36]. The band at 1630 cm^{-1} is assigned to short-segment chains connecting α-helical segments of BSA. The bands at 1681 and 1623 cm^{-1} are assigned to anti-parallel β-sheets, and parallel and anti-parallel β-sheets, respectively [37,38].

By applying the curve deconvolution method we found that BSA at pH 7.4 showed 65 ± 1% α-helix (peak at 1656 cm^{-1}), 18 ± 1%

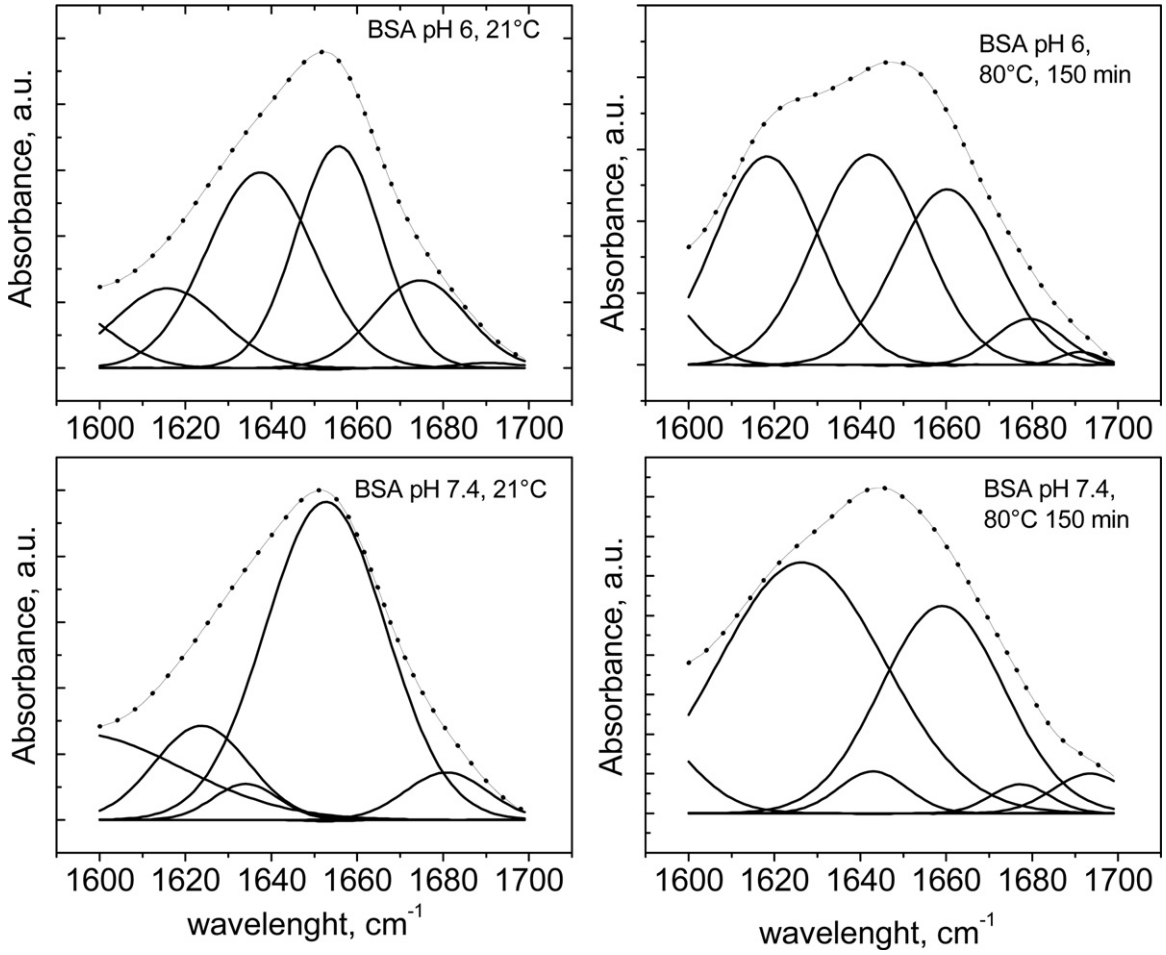

Fig. 5. FTIR spectra in the amide I region of 10 mg/mL BSA in 25 mM PBS, pH 6.0 or 7.4, analysed at $t = 0$ and after 150 min incubation at 80 °C, compared with the spectra reconstructed (bold dotted line). The single Gaussian components are also shown.

parallel β sheets (peak at 1623 cm^{-1}), 25 ± 1% turn structure and 3 ± 1% anti-parallel β-sheets. These percentages changed at pH 6.0. FTIR spectra showed a peak at 1609 cm^{-1} due to the vibrations of Gln and the aromatic side chain [39], representing 22%, the peak at 1633 cm^{-1} (23%), 1656 cm^{-1} (44%), 1675 cm^{-1} (3%) and 1695 cm^{-1} (6%). BSA did not show any structural change if incubated at room temperature (21 ± 1 °C) at pH 6.0 and 7.4 for a time tested of 150 min. The amide I band becomes broader after incubation at higher temperature, and additional bands due to aggregated and/or denatured species appeared.

Fig. 6 shows the temperature-dependent variations of the peak height intensity percentages of individual Gaussian components associated with the different secondary structures observed at pH 7.4 and 6.0 as a function of the incubation time at 60 and 80 °C.

At pH 7.4 BSA incubated at 60 °C (Fig. 6A) showed a decrease of α-helix peak at 1653 cm^{-1} from 65 to around 45%, an increase of turns at 1676 cm^{-1}, that reached 20%, and a decrease of anti-parallel β-sheet peak at 1681 cm^{-1}. These conformational changes, likely associated with pre-denatured states of BSA, were responsible for the increase of protein surface tension (Fig. 4B). At 80 °C (Fig. 6B) the α-helix peak decreased down to 20%, the peaks at 1634 cm^{-1} and 1676 cm^{-1} assigned to turn structures increased until 60 min incubation time. For longer incubation times (150 min) turn structures switched into parallel β-sheet structures (peak at 1623 cm^{-1}), and we observed an increase of "nominal" α-helix that shifted toward 1660 cm^{-1}.

On the basis of these results we can suggest that the increase of DSTD *plateau* signal (Fig. 4B) from 100 (DTSD peak area obtained at 21 °C) to 400 and 500 observed after more than 10 min incubation at 60 and 80 °C, respectively can be due to the BSA thermal denaturation with the increase of protein flexibility and the exposure to the solvent of protein hydrophobic patches. The increase of β-sheets is diagnostic for intra-peptide chain aggregation [40–42]. At 80 °C (Fig. 6B) this phenomenon was more evident, and gave also a shift of peak frequencies (Fig. 6B, inlet) toward higher values, which is consistent with a more hydrophobic environment: from 1681 to

Table 1
Intrinsic viscosity values found in this study and reported in the literature. The effective spherical radius (R_e) is also reported.

	Intrinsic viscosity [η] (mL/g)	Intrinsic viscosity [η] (mL/g)	R_e[a] (nm)
	This work	Literature	
BSA in 1 M PBS pH 7.4 (native)	3.18 ± 0.90	3.7–4.5 [49,50,51]	3.23 (this work) 3.42 [52]
BSA in 25 mM PBS pH 7.4 (native)	2.86 ± 0.56	3.71–4.12 [53]	3.11 (this work) 3.37 [53]
BSA denatured in 8 M urea, 50 mM PBS pH 7.4	25.7 ± 3.80	25.4 [54]	6.47 (this work) 6.27 [4] 7.53 [52]
BSA incubated at 80 °C for 150 min	3720 ± 550	–	34.0 (this work) 21–29 (heat-induced aggregates, various conditions) [55–57]

[a] R_e has been calculated on the basis of Eq. (4).

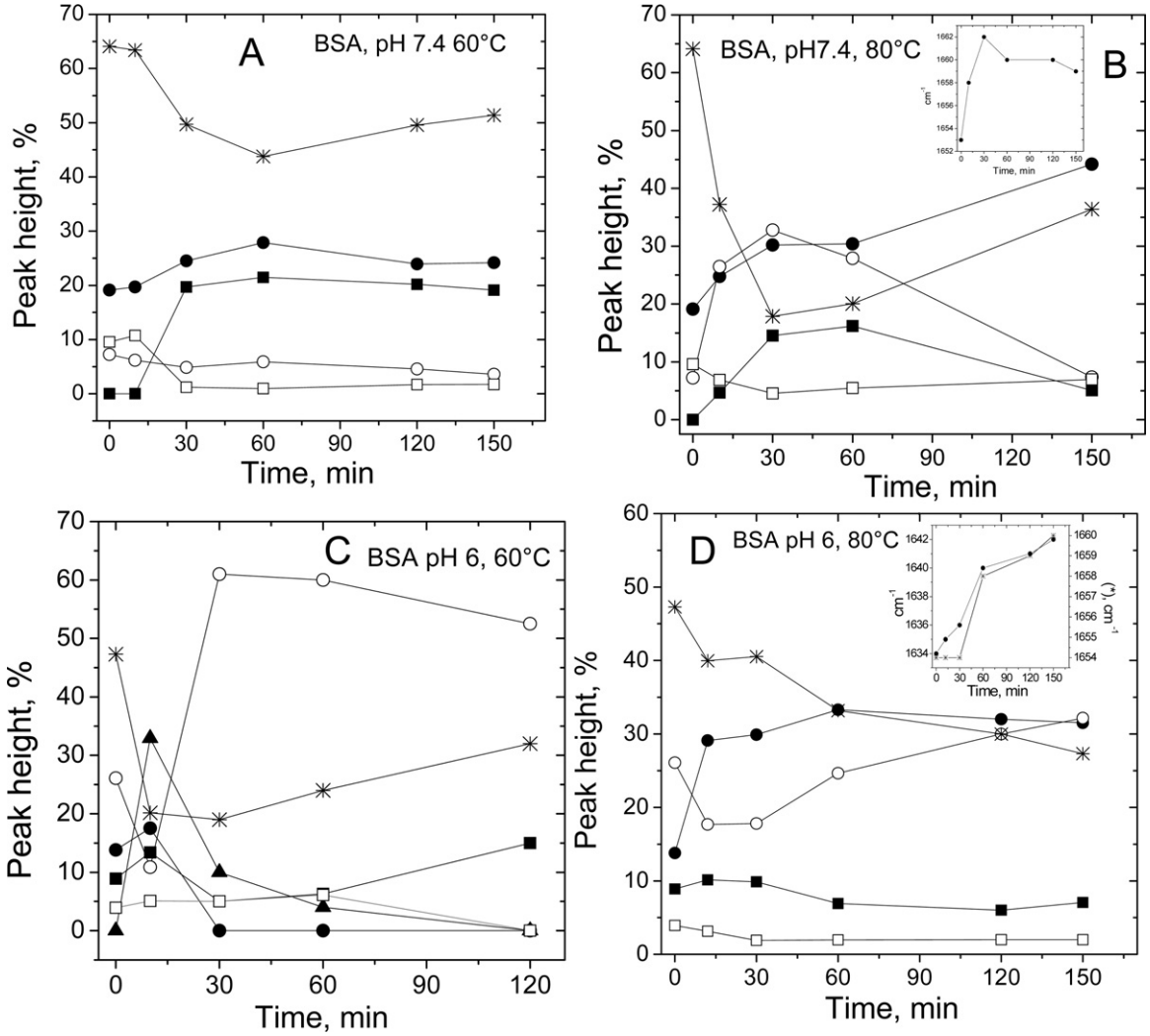

Fig. 6. Temperature dependences of the peak height intensity percentages of individual Gaussian components associated with the different secondary structures observed at pH 7.4 and 6.0 as a function of the incubation time at 60 and 80 °C: peak at 1615 cm^{-1} (at pH 6)/1623 (at pH 7.4) (filled circle); peak at 1634 cm^{-1} (open circle); peak at 1656 cm^{-1} (at pH 6)/1653 (at pH 7.4) (asterisk); peak at 1676 cm^{-1} (filled square); peak at 1687 cm^{-1} (at pH 6)/1681 (at pH 7.4) (open square); peak at 1646 cm^{-1} (filled triangle). Inlet plots show the shift of α-helix and turn structure peaks.

1690 cm^{-1} for anti-parallel β-sheets, from 1653 to 1660 cm^{-1} for α-helix peak. The frequency of turn structures at 1634 cm^{-1} shifted to 1645 cm^{-1}, a frequency typical of random structure [43].

No significant changes of BSA solution viscosity observed at 60 °C nor 80 °C at pH 7.4 (Fig. 4A). At pH 7.4 denaturation occurs, but inter-peptide protein aggregation phenomena are absent or modest. Surface activity increases because BSA molecules do not form big aggregates and maintain a good diffusion rate toward the drop surface. At pH 6.0, instead, a pH closer to the BSA isoelectric point (pI = 5.4), BSA molecules are more "sticky". All the albumins are indeed characterized by a maximum surface activity at acidic pH, with a peak around their isoelectric point (pH 4.5–5.0) [21]. The peak in correspondence with the p*I* can be attributed to the decreased electric barrier for adsorption, decreased repulsion in the interfacial layer, and minimum solubility of the protein in the bulk phase [44,45]. At high temperatures (80 °C) this property could favor an inter-molecular aggregation process and the formation of big aggregates that increase solution viscosity, but cannot diffuse to the drop surface (low surface tension value).

At pH 6, BSA incubated at 60 °C (Fig. 6C) showed a decrease of α-helix peak at 1656 cm^{-1} from 48 to about 20%, an increase of the peak at 1634 cm^{-1}, reaching 60% after 30 min incubation and a transient peak of a peak at 1646 cm^{-1}, assigned to random structure, after 10 min. Both peaks assigned to β-sheet structures decreased after incubation at 60 °C.

No significant variation of BSA solution viscosity was observed at 60 °C (Fig. 4C), but a transient increase of surface tension signal was observed after 10 min (Fig. 4D), correlated with the formation of the random coil.

At pH 6, BSA incubated at 80 °C (Fig. 6D) showed a decrease of α-helix (from 48 to 30%) accompanied by an increase in inter-molecular β-sheets from 14 to about 30%, characteristics of the aggregation process [46]. The peak position at 1615 cm^{-1} suggests the formation of the β-sheet structures with very strong hydrogen bond interactions leading to irreversible aggregation of the protein (named β-aggregation). The peak at 1634 cm^{-1} assigned to turns showed a decrease up to 30 min, but it increases for longer incubation time shifting toward 1642 cm^{-1}, frequency typical of random structures (Fig. 6 D, inlet). The α-helix peak shifted, as well, from 1654 cm^{-1} toward 1660 cm^{-1}, as observed also at pH 7.4.

The mechanism by which gels are formed when proteins such as BSA are heated has been established [47]. This thermally induced

gelation is a two-stage sequential process. The first phase involves heat-induced conformational changes in the protein with unfolding of some polypeptide segments [48]. Exposure of hydrophobic groups results in hydrophobic interactions that are preliminary to the subsequent phase of protein–protein interactions. This process results in a progressive buildup of a cross-linked gel network [49,50].

These conformational changes help to explain the increase of BSA solution viscosity (Fig. 4C), due to β-aggregation, as well as the disappearance of DSTD signal (Fig. 4D), due to the slow diffusion of large aggregates to the drop surface during the drop time ("analytical window").

3.3. Determination of the molecular size of denatured and aggregated species

Intrinsic viscosity of native and denatured BSA measured using the SCV was used for the calculation of the molecular size of denatured and aggregated species. Table 1 summarizes intrinsic viscosity data and the effective spherical radius (R_e) for native BSA and BSA denatured by 8 M urea and heat (150 min incubation at 80 °C) obtained in this work, compared with the literature data.

The good agreement of the values found in this work with those reported in the literature suggests a reliable employment of DSTD-SCV device also for the characterization of proteins in clinical samples and biotechnological processes.

4. Conclusions

The SCV detector presented herein is easily constructed, gives accurate and reliable measurements over a wide range of viscosities and provides an added value for the DSTD measurements. The SCV detector, as well as DSTD, uses a small volume of analyte (50–200 μL loop depending on the application considered). It can be easily cleaned and employed for materials with biological hazard.

We envision this approach can be used for the study of protein aggregation processes and of the effects of substances affecting aggregation (*e.g.* metal ions, sugars or polyphenols) [51–53]. These processes are of particular interest in food technology and biomaterials [54].

In the specific application to BSA, the simultaneous measurement of surface tension and viscosity allowed us to observe that temperature-induced denaturation of BSA has different effects depending on the pH of solution. In summary, at pH 7.4 BSA showed an increase of surface tension with small variation of solution viscosity, accompanied by structural changes (at 80 °C more significant than at 60 °C), which include a decrease of α-helix structure and an increase of β-sheets and turns. These results suggest the formation of denatured protein molecules and/or small aggregates, rich of β-sheet structures and of surface hydrophobic patches responsible for the increase of surface activity. However at this pH the repulsion forces due to the positive net charge of the protein avoids the formation of big aggregates. At pH 6, a pH which is closer to BSA isoelectric point, it is likely to hypothesize that the increase of surface hydrophobicity due to temperature-induced denaturation is accompanied also by inter-peptide electrostatic interactions that favor the formation of larger β-sheet structured aggregates.

Acknowledgements

The authors would like to acknowledge Dr Elpidio Tombari for his helpful discussion in setting up SCV detector. This work has been financially supported by PRIN 2008 funding from Italian Ministry of University and Research (Project No. 2008XXAMZT).

Appendix A. Supplementary data

Supplementary data associated with this article can be found, in the online version, at doi:10.1016/j.talanta.2011.08.009.

References

[1] M. El-Nokaly, D. Cornell, Microemulsions and Emulsions in Foods, American Chemical Society, Washington, DC, 1991.
[2] T.F. Tadros, Surfactants in Agrochemicals, Marcel Dekker, New York, 1997.
[3] B. Vardhanabhuti, E.A. Foegeding, Journal of Agricultural and Food Chemistry 47 (1999) 3649–3655.
[4] S. Choi, J.K. Park, Small 6 (2010) 1306–1310.
[5] A.P. Froba, A. Leipertz, International Journal of Thermophysics 24 (2003) 895–921.
[6] H. Fujii, F. Matsumoto, T. Ueda, K. Nogi, Journal of Materials Science 40 (2005) 2161–2166.
[7] W.K. Rhim, K. Ohsaka, P.F. Paradis, R.E. Spjut, Review of Scientific Instruments 70 (1999) 2796–2801.
[8] M. Singh, Surface and Interface Analysis 40 (2008) 1344–1349.
[9] M. Singh, Journal of Applied Polymer Science 110 (2008) 2293–2304.
[10] M. Singh, Surface and Interface Analysis 40 (2008) 15–21.
[11] L.R. Lima, D.R. Dunphy, R.E. Synovec, Analytical Chemistry 66 (1994) 1209–1216.
[12] L.R. Lima, R.E. Synovec, Journal of Chromatography A 691 (1995) 195–204.
[13] N.A. Olson, R.E. Synovec, W.B. Bond, D.M. Alloway, K.J. Skogerboe, Analytical Chemistry 69 (1997) 3496–3505.
[14] T.E. Young, R.E. Synovec, Talanta 43 (1996) 889–899.
[15] K.E. Miller, K.J. Skogerboe, R.E. Synovec, Talanta 50 (1999) 1045–1056.
[16] N.A. Olson, K.J. Skogerboe, R.E. Synovec, Journal of Chromatography A 806 (1998) 239–250.
[17] K.E. Miller, E. Bramanti, B.J. Prazen, M. Prezhdo, K.J. Skogerboe, R.E. Synovec, Analytical Chemistry 72 (2000) 4372–4380.
[18] K.E. Miller, R.E. Synovec, Analytica Chimica Acta 412 (2000) 149–160.
[19] E. Bramanti, C. Allegrini, M. Onor, G. Raspi, K.J. Skogerboe, R.E. Synovec, Analytical Biochemistry 351 (2006) 100–113.
[20] W.W.C. Quigley, E. Bramanti, B.A. Staggemeier, K.E. Miller, A. Nabi, K.J. Skogerboe, R.E. Synovec, Analytical and Bioanalytical Chemistry 378 (2004) 134–143.
[21] B.A. Staggemeier, E. Bramanti, C. Allegrini, K.J. Skogerboe, R.E. Synovec, Analytical Chemistry 77 (2005) 250–258.
[22] F.B. Malihi, C. Kuo, M.E. Koehler, T. Provder, A.F. Kah, Development of a continuous gel permeation chromatography viscosity detector for the characterization of absolute molecular weight distribution of polymers, in: T. Provder (Ed.), Size Exclusion Chromatography, American Chemical Society, 1984, pp. 281–294.
[23] E. Bramanti, W.W.C. Quigley, C. Sortino, F. Beni, M. Onor, G. Raspi, R.E. Synovec, Journal of Chromatography A 1023 (2004) 79–91.
[24] R.C. Weast, Handbook of Chemistry and Physics: A Ready-Reference Book of Chemical and Physical Data, Chemical Rubber Co., 1967.
[25] C. Tanford, Physical Chemistry of Macromolecules, John Wiley & Sons, Inc., New York, 1961.
[26] E. Bramanti, M. Bramanti, P. Stiavetti, E. Benedetti, Journal of Chemometrics 8 (1994) 409–421.
[27] E. Bramanti, E. Benedetti, Biopolymers 38 (1996) 639–653.
[28] Y.N. Chirgadze, O.V.T.N.P Fedorov, Biopolymers (1975) 679–694.
[29] N.E. Dorsey, Properties of Ordinary Water Substance, Reinhold, New York, 1940.
[30] P. Huibers, A Review of Nonionic Surfactant Micellar Kinetics Studies Using the Temperature-Jump Technique, Department of Chemical Engineering, University of Florida, Gainesville, FL, 1996.
[31] B.A. Staggemeier, T.O. Collier, B.J. Prazen, R.E. Synovec, Analytica Chimica Acta 534 (2005) 79–87.
[32] D.C. Carter, J.X. Ho, Advances in Protein Chemistry 45 (1994) 153–203.
[33] K. Murayama, M. Tomida, Biochemistry 43 (2004) 11526–11532.
[34] J.F. Foster, in: V.M. Rosenoer, M. Oratz, M.A. Rothschild (Eds.), Albumin Structure, Function and Uses, Pergamon, Oxford, 1977.
[35] B. Jachimska, M. Wasilewska, Z. Adamczyk, Langmuir 24 (2008) 6866–6872.
[36] H. Fabian, W. Mantele, Infrared Spectroscopy of Proteins, John Wiley and Sons, Chichester, 2002.
[37] Y.N. Chirgadze, N.A. Nevskaya, Biopolymers 15 (1976) 607–625.
[38] S. Krimm, J. Bandekar, Advances in Protein Chemistry 38 (1986) 181–364.
[39] H.L. Casal, U. Kohler, H.H. Mantsch, Biochimica et Biophysica Acta 957 (1988) 11–20.
[40] T. Lefevre, M. Subirade, Biopolymers 54 (2000) 578–586.
[41] A.A. Ismail, H.H. Mantsch, P.T.T. Wong, Biochimica et Biophysica Acta 1121 (1992) 183–188.
[42] D.M. Byler, H. Susi, Biopolymers 25 (1986) 469–487.
[43] H. Susi, D.M. Byler, Methods in Enzymology 130 (1986) 290–311.
[44] S. Magdassi, A. Kamyshny, Surface Activity of Proteins: Chemical and Physiochemical Modifications, Marcel Dekker, New York, 1996.

[45] J.R. Lu, T.J. Su, J. Penfold, Langmuir 15 (1999) 6975–6983.
[46] A.H. Clark, D.H.P. Saunderson, A. Suggett, International Journal of Peptide Protein Research (1981) 353–364.
[47] S.F. Edwards, P.J. Lillford, J.M.V. Blanshard, Food Structure and Behaviour, Academic Press, New York, 1987.
[48] S. Damodaran, Interrelationship of Molecular and Functional Properties of Food Proteins, American Oil Chemists' Society, Champaign, IL, 1989.
[49] S. Damodaran, Structure–Function Relationship of Food Proteins, Elsevier Applied Science, New York, 1994.
[50] V. Bernal, P. Jelen, Journal of Dairy Science 68 (1985) 2847–2852.
[51] G. Navarra, D. Giacomazza, M. Leone, F. Librizzi, V. Militello, P.L.S. Biagio, European Biophysics Journal 38 (2009) 437–446.
[52] G. Navarra, A. Tinti, M. Leone, V. Militello, A. Torreggiani, Journal of Inorganic Biochemistry 103 (2009) 1729–1738.
[53] P. Rondeau, G. Navarra, F. Cacciabaudo, M. Leone, E. Bourdon, V. Militello, Biochimica et Biophysica Acta: Proteins and Proteomics 1804 (2010) 789–798.
[54] R. Rohanizadeh, N. Kokabi, Journal of Materials Science. Materials in Medicine 20 (2009) 2413–2418.
[55] R. Su, W. Qi, Z. He, Y. Zhang, F. Jin, Food Hydrocolloids 22 (2008) 995–1005.
[56] G. Yohannes, S.K. Wiedmer, M. Elomaa, M. Jussila, V. Aseyev, M.-L. Riekkola, Analytica Chimica Acta 675 (2010) 191–198.
[57] V. Militello, C. Casarino, A. Emanuele, A. Giostra, F. Pullara, M. Leone, Biophysical Chemistry 107 (2004) 175–187.